IEEE Access
Multidisciplinary ⋮ Rapid Review ⋮ Open Access Journal

Received April 9, 2019, accepted May 21, 2019, date of publication June 14, 2019, date of current version July 2, 2019.

Digital Object Identifier 10.1109/ACCESS.2019.2923166

Synthesis and Optimization of Fractional-Order Elements Using a Genetic Algorithm

ASLIHAN KARTCI[1,2], (Student Member, IEEE), AGAMYRAT AGAMBAYEV[3], MOHAMED FARHAT[3], NORBERT HERENCSAR[2], (Senior Member, IEEE), LUBOMIR BRANCIK[1], (Senior Member, IEEE), HAKAN BAGCI[3], (Senior Member, IEEE), AND KHALED N. SALAMA[3], (Senior Member, IEEE)

[1]Department of Radio Electronics, Brno University of Technology, 616 00 Brno, Czech Republic
[2]Department of Telecommunications, Brno University of Technology, 616 00 Brno, Czech Republic
[3]Computer, Electrical and Mathematical Sciences & Engineering Division, King Abdullah University of Science and Technology, Thuwal 23955, Saudi Arabia

Corresponding author: Aslihan Kartci (kartci@feec.vutbr.cz)

Research described in this paper was supported by the King Abdullah University of Science and Technology, Saudi Arabia, the National Sustainability Program under grant LO1401, the Ministry of Education, and the Czech Science Foundation under grant no. 19-24585S. For the research, infrastructure of the SIX Center was used.

ABSTRACT This study proposes a new approach for the optimization of phase and magnitude responses of fractional-order capacitive and inductive elements based on the mixed integer-order genetic algorithm (GA), over a bandwidth of four-decade, and operating up to 1 GHz with a low phase error of approximately $\pm 1^{\circ}$. It provides a phase optimization in the desired bandwidth with minimal branch number and avoids the use of negative component values, and any complex mathematical analysis. Standardized, IEC 60063 compliant commercially available passive component values are used; hence, no correction on passive elements is required. To the best knowledge of the authors, this approach is proposed for the first time in the literature. As validation, we present numerical simulations using MATLAB® and experimental measurement results, in particular, the Foster-II and Valsa structures with five branches for precise and/or high-frequency applications. Indeed, the results demonstrate excellent performance and significant improvements over the Oustaloup approximation, the Valsa recursive algorithm, and the continued fraction expansion and the adaptability of the GA-based design with five different types of distributed RC/RL network.

INDEX TERMS Cauer network, constant phase element, continued fraction expansion, distributed RC network, distributed RL network, Foster network, fractional-order capacitor, fractional-order element, fractional-order inductor, genetic algorithm, impedance optimization, phase optimization, RC network, RL network, recursive algorithm, Valsa network.

I. INTRODUCTION

Recently, tremendous efforts have been made to design fractional-order elements (FOEs). Indeed they offer additional degrees of freedom and versatility in electrical circuits [1]–[4], such as filters [5]–[7], oscillators [8]–[11], controllers [12]–[15], bioimpedance modeling [16], lithium-ion battery modeling [17], transmission line design [18], reluctance inductive transducer realization [19], dc–dc boost converters [20] and references cited therein. The versatility of fractional-order circuits leads researchers to believe that the future of discrete element circuit design will undergo a paradigm shift in favor of FOEs [21]. Fig. 1 shows the fundamental components and possible FOEs in four quadrants [22], [23]. Their impedance is described as $Z(s) = Ks^{\alpha}$, where ω is the angular frequency in $s = j\omega$, and obviously has a real part dependent on the non-zero frequency. In particular, the impedance of Type IV FOEs, i.e. fractional-order capacitors (FOCs), is provided with an order of $-1 < \alpha < 0$ and pseudocapacitance of $C_{\alpha} = 1/K$, whereas fractional-order inductors (FOIs) in quadrant I (Type I) have an order of $0 < \alpha < 1$ and pseudoinductance of $L_{\alpha} = K$. These two FOEs are the key components in fractional-order circuit design and our main object of investigation in this work. Their characteristics such as pseudocapacitance, pseudoinductance, constant phase zone (CPZ), constant phase angle (CPA – defined phase

The associate editor coordinating the review of this manuscript and approving it for publication was Hisao Ishibuchi.

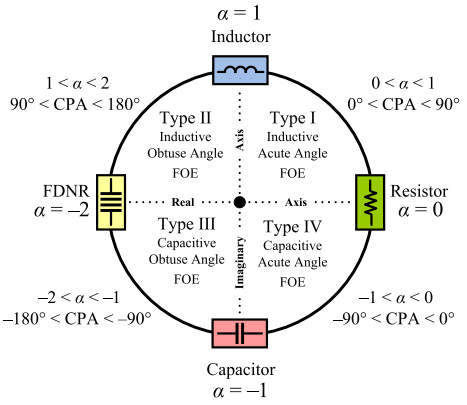

FIGURE 1. Description of fractional-order elements in four quadrants [22], [23].

angle in CPZ), and phase angle deviation (PAD – maximum difference between a designed/measured phase and a target phase) profoundly impact the transfer function of those systems [1], [2], [4], [22].

Different approaches to the realization of an FOC using dielectric materials [24]–[27], a liquid electrochemical capacitor [28], [29], and other active emulators [30] exist in the open literature. However, they are in the conceptual stage and still require much work before they meet the expectations of circuit designers. One method of implementing an FOC is to approximate the rational function of s in a desired bandwidth using the methods of Carlson [31], Matsuda [32], El-Khazali [33], Maione [34], Oustaloup [35], Continued Fraction Expansion (CFE) [36], and Recursive Algorithms (RAs) [37], [38] among others [39]–[43]. Once a rational function is obtained, it can be synthesized by the use of a weighted sum of first-order filter sections [44], active building blocks [45], controllers [46], bilinear sections [47], tree structures [48], RC ladder networks [36], or a Valsa structure [37]. Subsequently, by defining the C_α, their overall transfer function mimics the impedance of FOCs at a specific frequency range. On the other hand, there are few approaches that mimic the FOI response such as RL-networks [20], equiripple and El-Khazali approximations [33], using generalized impedance converters (GICs) [19], [23], [23], [49]–[52], or other active emulators [45]–[47]. However, the trade-off between an operating frequency range and the number of circuit elements required in the FOC or FOI design limits the use of passive or active emulators in many applications. In addition, all above mentioned approximation methods are analytical and require not standard IEC 60063 compliant values of resistors, capacitors, and inductors to have better results. If the used values are replaced by the closest standardized values, the accuracy of the approximation decreases, which leads to an increase of PAD and overall degradation of the performance of the FOE (for instance [15], [20], [23]).

Up until now, evolutionary computing algorithms have been used to reduce the drawbacks in traditional optimization methods and to solve complex problems where conventional techniques fail in many areas of the fractional-order domain such as chaos [53], control [54], or extracting the design parameters of filters [55]. In this regard, flower pollination algorithms [56], particle swarm optimization [57], or genetic algorithms (GA) [58] are used. In this work, a mixed integer-order GA in MATLAB® is used. Instead of approximating s^α using the above mentioned approximations at a certain frequency (or bandwidth), we optimize the phase and/or magnitude responses of RC/RL networks in the whole desired frequency range. In brief, the GA is a powerful computational technique, which mimics the process of natural selection theory. It consists of a population of representations of candidate solutions to an optimization problem, which evolve toward enhanced solutions. It is important to mention that the GA uses the objective function itself, not derivatives or other auxiliary knowledge based on probabilistic/deterministic characterization. These features make this optimization method the most suitable technique to optimize the CPA in distributed RC/RL networks. Furthermore, the required values are obtained with GA, even if the passive component values are restricted to commercially available kit values defined by standard IEC 60063, and still maintain superb results. Hence, the paper aims to introduce an FOE optimization method that achieves a broad operating frequency range with CPA deviation of approximately $\pm 1^\circ$ using commercially available passive component values in RC and RL structures with five branches of Foster-I, Foster-II, Cauer-I, Cauer-II, and Valsa networks. Most crucially, the presented approach avoids the use of negative component values, GICs, or random passive element values. Thus, this article deals with the optimal emulation of an FOE currently available in the literature. In particular, Foster-II and Valsa networks are selected as our main objective, because the former offers a minimum total capacitance value and the latter provides a minimum CPA deviation. Here it is also worth noting that, to the best knowledge of authors, an FOI design using the listed five RL networks is studied for the first time in the literature.

The rest of this work is organized as follows. Section II describes the proposed optimization approach using GA as well as design considerations. In Section III, five types of RC networks for FOC design with optimized passive component values are analyzed numerically and the particular cases experimentally. Furthermore, the FOC results of comparisons with other algorithms (CFE, Oustaloup, and RA) are presented. A numerical study of FOI with five types of RL networks using GA is presented for the first time in the literature in the Section IV. As an example, the behavior of the optimized Valsa structure is measured. Section V discusses the results and performance characteristics of all examples, whereas the Section VI concludes the study.

II. DESCRIPTION OF THE GA APPROACH USED IN OPTIMIZATION OF FOE

Table 1 summarizes the FOC and FOI approximation methods used in this work with their synthesized RC and RL net-

TABLE 1. FOC and FOI approximation methods used in this study (note: all below networks are optimized using GA).

FOC Approximation			FOI Approximation		
Method	Admittance, $Y(s)$	RC Network	Method	Impedance, $Z(s)$	RL Network
Oustaloup	$Ck_f \sum_{i=1}^{n} \frac{1+(s/\omega_i')}{1+(s/\omega_i)}$ [35]	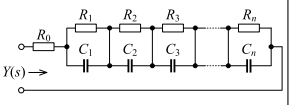 Foster-I	GA	$R_0 + \sum_{i=1}^{n} \frac{sL_iR_i}{R_i+sL_i}$	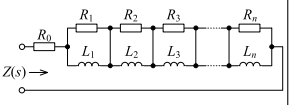 Foster-I
CFE	$\frac{1}{R_0} + \sum_{i=1}^{n} \frac{sC_i}{sC_iR_i+1}$	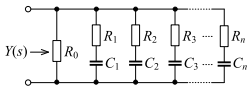 Foster-II	GA	$\frac{1}{\frac{1}{R_0} + \sum_{i=1}^{n} \frac{1}{R_i+sL_i}}$	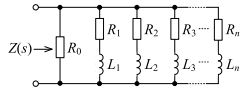 Foster-II
CFE	$R_1 + \frac{1}{sC_1+} \frac{1}{R_2+} \frac{1}{sC_2+} \cdots \cdots \frac{1}{sC_n+} \frac{1}{R_0}$	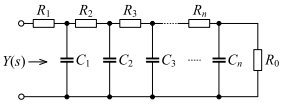 Cauer-I	GA	$R_1 + \frac{1}{\frac{1}{sL_1}+} \frac{1}{R_2+} \frac{1}{\frac{1}{sL_2}+} \cdots \cdots \frac{1}{\frac{1}{sL_n}+} \frac{1}{R_0}$	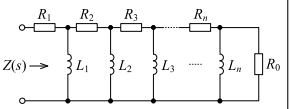 Cauer-I
CFE	$\frac{1}{\frac{1}{R_1}+} \frac{1}{\frac{1}{sC_1}+} \frac{1}{\frac{1}{R_2}+} \frac{1}{\frac{1}{sC_2}+} \cdots \cdots \frac{1}{\frac{1}{sC_n}+} R_0$	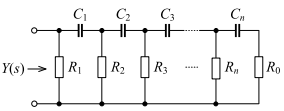 Cauer-II	GA	$\frac{1}{\frac{1}{R_1}+} \frac{1}{sL_1+} \frac{1}{\frac{1}{R_2}+} \frac{1}{sL_2+} \cdots \cdots \frac{1}{sL_n+} R_0$	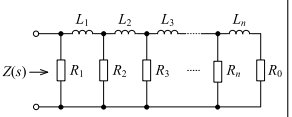 Cauer-II
RA	$\frac{1}{R_0} + sC_0 + \sum_{i=1}^{n} \frac{sC\varepsilon^i}{sCR+(\eta\varepsilon)^i}$ [37], [38] Note: η is capacitance and ε is resistance scaling factors	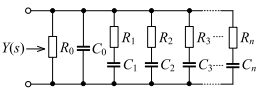 Valsa	GA	$\frac{1}{\frac{1}{R_0} + \frac{1}{sL_0} + \sum_{i=1}^{n} \frac{1}{R_i+sL_i}}$	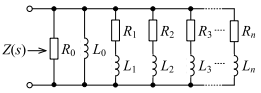 Valsa

Algorithm 1 Genetic Algorithm Pseudocode

1: **for** $i = 1$ to *NumOfGenerations* (or until an acceptable solution is found) **do**
2: **if** first generation **then**
3: Generate the initial population with primitives (CPZ, CPA, pseudocapacitance, pseudoinductance, number of branches, resistor, capacitor, and inductor set)
4: **else**
5: With current population, generate a new one using crossover and mutation operators
6: **end if**
7: Calculate fitness of population members
8: **if** fitness $\neq 0$ **then**
9: Return to generate new population
10: **else**
11: Break the loop
12: **end if**
13: **end for**
Return best individual in last population

works and equivalent admittances or impedances. The admittances of some of the RC networks can be found in [4], [36]. The impedance and phase optimization of all structures using the GA is obtained with predefined R and C values. The desired constant phase and/or pseudocapacitance, pseudoinductance, number of branches, and frequency range (i.e. CPZ) are defined as design parameters.

To provide more detail regarding the exact steps that were performed by the GA approach, we present its pseudocode in

TABLE 2. Genetic algorithm parameters.

Run Parameter	Value
Population size	100
Max. stall generation	125
Max. generation	10 000
Input variables	6
Crossover probability	0.5
Random range of resistor values (Ω)	1 – 10 M (in total, 1 000 points divided into n logarithmically equal sections are used)
Random range of capacitor values (F)	1 f – 1 μ (in total, 1 000 points divided into n logarithmically equal sections are used)
Commercially available resistor kits	YAGEO RC-0603-FR-07 E96 Kit [59] and Vishay 0402 [60]
Commercially available capacitor kits	muRata C0603 [61] and Kemet 0402 [62]
Commercially available inductor kit	Coilcraft 0603 ceramic inductors [63]

Algorithm 1 based on [58]. Table 2 presents the parameters employed during the training phase of the GA approach. Fitness, also known as the cost function of the solution set, is determined using the following equation:

$$F = \left|\varphi_{\text{sim}} - \varphi_{\text{targ}}\right|, \tag{1}$$

where φ_{sim} and φ_{targ} express the simulated and target phase, respectively.

III. OPTIMIZATION AND VERIFICATION OF FOC

As an exemplary study, primarily the Foster-II [36] and Valsa [37] networks are optimized within this section. For the reason that; Foster-II network offers a minimum total capacitance value and Valsa network provides a minimum PAD.

A. OPTIMIZATION OF FOSTER-II STRUCTURE FOR FOC DESIGN

For a Foster-II realization, the component values are given by the partial fraction expansion and its admittance is expressed in Table 1. Here, n is the number of branches, R_0 is the initial resistor, and R_i and C_i are the resistances and capacitances of i-th branch. Firstly, the performance of the network obtained using the GA with the Oustaloup and CFE methods is compared to show the advantage of the GA. The desired bandwidth, number of branches which is equivalent of a fifth-order admittance function ($n = 5$), and CPA are respectively set as 100 Hz−1 MHz, 5, and −45° with a pseudocapacitance of $C_\alpha = 100$ nF·s$^{-0.5}$. As a population, the random and commercially available passive elements defined in Table 2 are used. The central frequency in case of CFE is set to 10 kHz. It can be observed from Fig. 2(a) that all three approximations provide a constant phase response with target CPA near a central frequency, specifically between 1 kHz and 100 kHz. However, errors in phase for the approximation models increase significantly when the frequency is 2 decades above and below the central frequency, whereas the phase response obtained using the GA is satisfied in the whole frequency range of interest. Furthermore, Fig. 2(b) shows relative phase errors and corresponding normalized histograms (%) of phase angle deviation from CPA as an inset. It can be seen that the maximum deviation in the GA is limited to only ±2°, whereas in both CFE and Oustaloup, ±25° errors occur. Because no direct control exists over the R and C values obtained from the last two approximations, a correction to use the commercially available RC kit values is obligatory to build the FOCs. However, this correction is not needed for the results obtained by the GA since it directly provides the standard IEC 60063 compliant RC values as the results. Indeed, it is possible to include in the population, i.e. available R and C values to MATLAB® and the GA performs the optimization using only given values. Fig. 2(c) shows the simulated phase response of corrected RC network values using the Oustaloup, CFE, and optimized network using the GA, while the commercially available 0603 size R and C kit values defined in Table 2 are used. The rest of

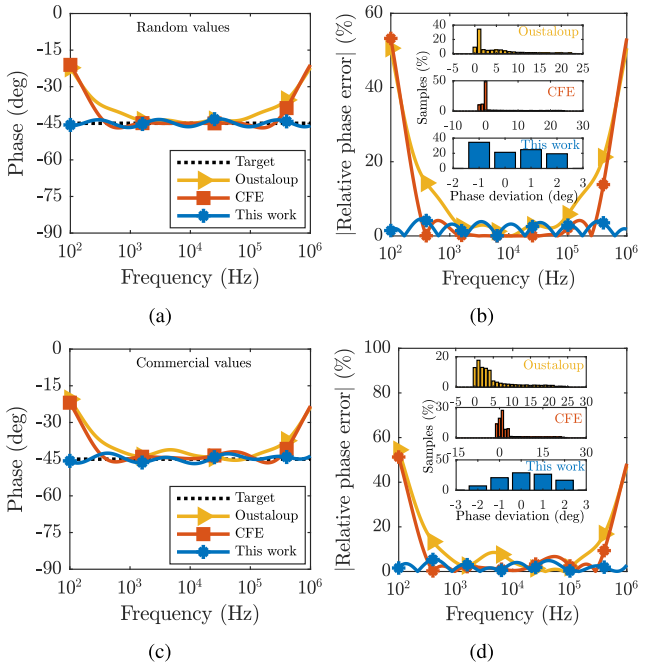

FIGURE 2. (a) Numerical phase response plots of the Foster-II RC network using the Oustaloup, CFE, and GA methods with random values, (b) relative phase errors and corresponding normalized histograms (%) of phase angle deviation from CPA as inset, (c) phase angle response of the RC network using the Oustaloup and CFE methods after RC value correction, and the GA optimized for commercially available RC kit values, (d) relative phase errors and corresponding normalized histograms (%) of phase angle deviation from CPA as inset. Phase responses are optimized in the frequency range of 100 Hz–1 MHz.

the simulation setup is identical to the simulation setup for Fig. 2(a). Fig. 2(d) plots the relative phase errors and corresponding normalized histograms (%) of phase angle deviation from CPA as an inset. As it can be observed, the maximum deviation in the GA is limited to ±2.8°, whereas ±30° error is obtained in both Oustaloup and CFE approximation results. Notably, the maximum error in the phase obtained from both approximation methods are further increased compared with the results in Fig. 2(b) with no RC value correction. However, no significant change is observed in the phase of the circuit obtained using the GA.

Figs. 3(a) and (c) show the target, simulated, and measured phase angle and pseudocapacitance responses of the RC network optimized using the GA. The same passive element values are used from the commercially available RC kits as depicted in Fig. 2(c) (see "This work") with the setup listed in Appendix A. The experimental verification uses the Agilent 4294A Precision Impedance Analyzer. Standard calibration tests (open and short circuits) of the Keysight 16048G Test Leads are performed to calibrate the instrument. From the results in Figs. 3(b) and (d), it can be seen that the maximum CPA deviation between target (ideal) and simulated as well as measured values is only ±2.8° and ±3.2°, respectively, whereas the pseudocapacitance is ±6.6 nF·s$^{-0.5}$ and ±7.3 nF·s$^{-0.5}$.

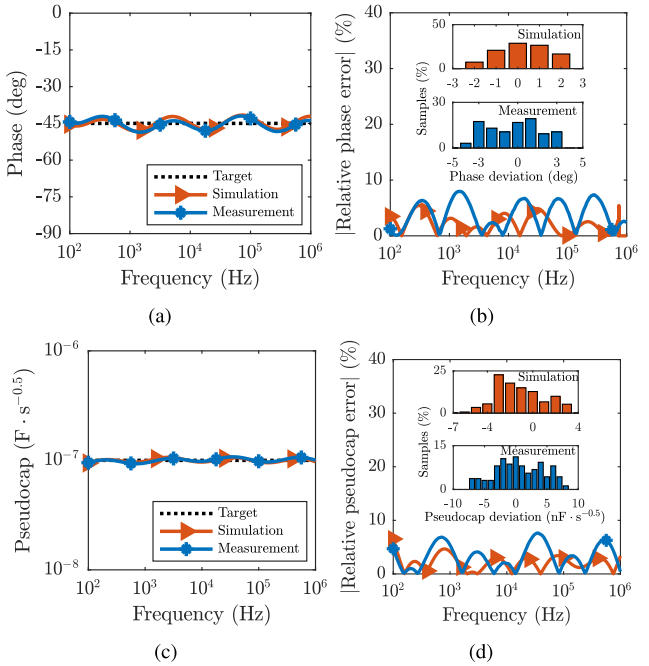

FIGURE 3. Target (ideal), simulated, and measured (a) phase responses, (b) relative phase errors and corresponding normalized histograms (%) of phase angle deviation from CPA as an inset, (c) pseudocapacitance responses, and (d) relative pseudocapacitance errors and corresponding normalized histograms (%) of pseudocapacitance deviation from CPA as an inset, respectively, of the Foster-II network optimized using GA. Impedance and phase responses are optimized in the frequency range of 100 Hz–1 MHz.

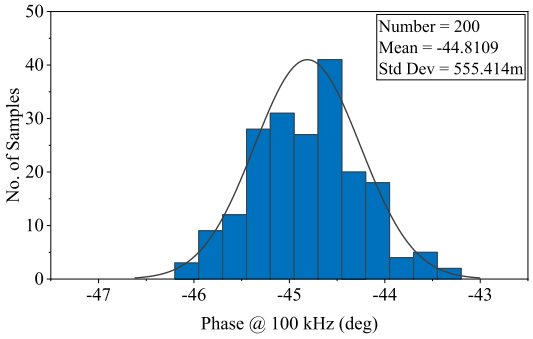

FIGURE 4. Monte Carlo analysis: Phase variation at 100 kHz of the Foster-II network optimized using GA (values used in Fig. 3(a)).

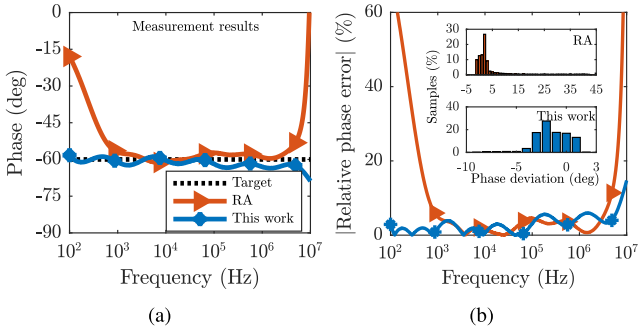

FIGURE 5. (a) Measured phase responses of the Valsa structure using the RA and GA methods (commercially available kits are used), and (b) relative phase errors and corresponding normalized histograms (%) of phase angle deviation from CPA as an inset. Impedances are measured in the frequency range of 100 Hz–10 MHz.

Statistical analysis of Monte Carlo (MC) was performed in OrCAD PSpice® simulation software with passive element tolerances based on their datasheets [59], [61] and 200 runs to observe effects due to manufacturing processes. The histogram shown in Fig. 4 demonstrates the variation of the phase at 100 kHz of the Foster-II network optimized using GA. The mean value with standard deviation 0.555 is $-44.8109°$, which is very close to the theoretical value $-45°$ confirming that the proposed network has low sensitivity characteristic on passive components. The analysis results of MC for all studied networks at their middle frequency are listed in Appendix A.

B. OPTIMIZATION OF VALSA STRUCTURE FOR FOC DESIGN

The Valsa network in Table 1 [37] is proposed to emulate FOC behavior and realized using RA. The possibility of designing this network using commercially available R and C values was claimed by the authors [37]. However, the RA allows us to set only initial values and the remaining branch values must be adjusted according to commercially available passive element values. With this in mind, similar to with the Foster-II structure, the GA is applied to the Valsa network in this subsection. The admittance function is given in Table 1, where compared to Foster-II network the additional C_0 denotes an initial capacitor. In our study, to provide a fair comparison with [37], the phase responses of RA and the GA of an order of $\alpha = -0.67$ using commercially available 0603 size RC kit values are experimentally evaluated. The used passive element values are listed in Appendix B (see "Fig. 5" columns). During the experimental verification, the same instruments listed in Section III(A) are used. With the phase error equal to $\pm 2.1°$, the approximation with the GA experimentally reaches a wider bandwidth of 100 Hz $-$ 5 MHz, as shown in Fig. 5(a). Considering the full frequency band up to 10 MHz, the error is still only $\pm 3.2°$ (see Fig. 5(b)).

Furthermore, the measurement results of $\alpha = -0.5$ order FOCs using an ENA Series Network Analyzer E5071C (300 kHz $-$ 20 GHz) in three different frequency ranges [case study (a) in 1 MHz $-$ 100 MHz, (b) 5 MHz $-$ 500 MHz, and (c) 50 MHz $-$ 1 GHz] are shown in Fig. 6. Two variants of the FOE device with dimensions of 20 mm $\times$ 20 mm were designed (for 0402 and 0603 size passive components) employing a subminiature version A (SMA) coaxial RF connector. The fabricated printed circuit board for 0402 size kit values is shown in Fig. 6(c) as an inset. Considering an input impedance 50 Ω of the connector, the phase is measured by defining the equation of impedance as $Z = 50 \cdot [(1 + S_{11})/(1 - S_{11})]$. As passive elements, RF-type resistors from Vishay [60] and capacitors from Kemet [62] are used. Because of the producers fabrication boundaries, used passive components having CPA in limited frequency

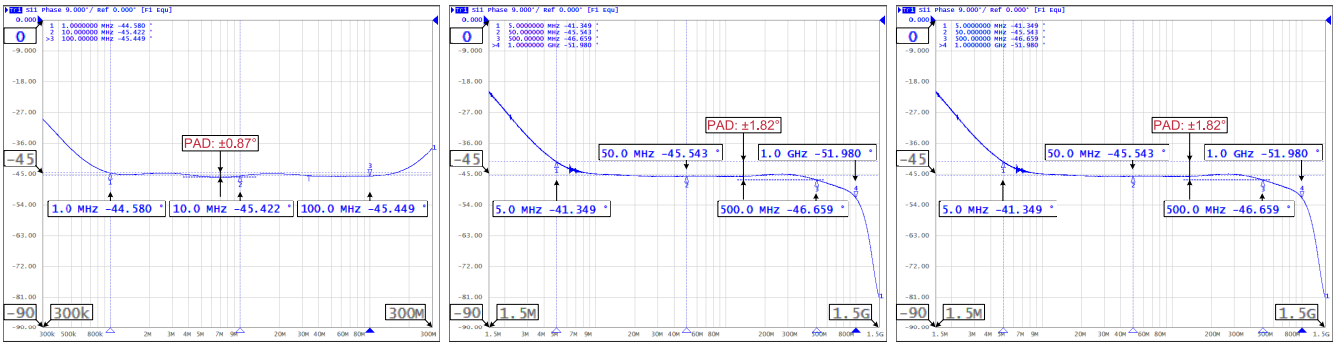

(a) (b) (c)

FIGURE 6. Measurement results of an $\alpha = -0.5$ order FOC implemented using the Valsa network optimized using GA for two decades in different frequency ranges: (a) 1 MHz–100 MHz, (b) 5 MHz–500 MHz, and (c) 50 MHz–1 GHz.

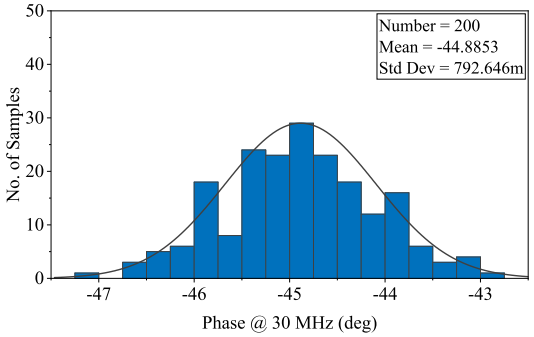

FIGURE 7. Monte Carlo analysis: Phase variation at 30 MHz of the Valsa network optimized using GA (values used in Fig. 6(a)).

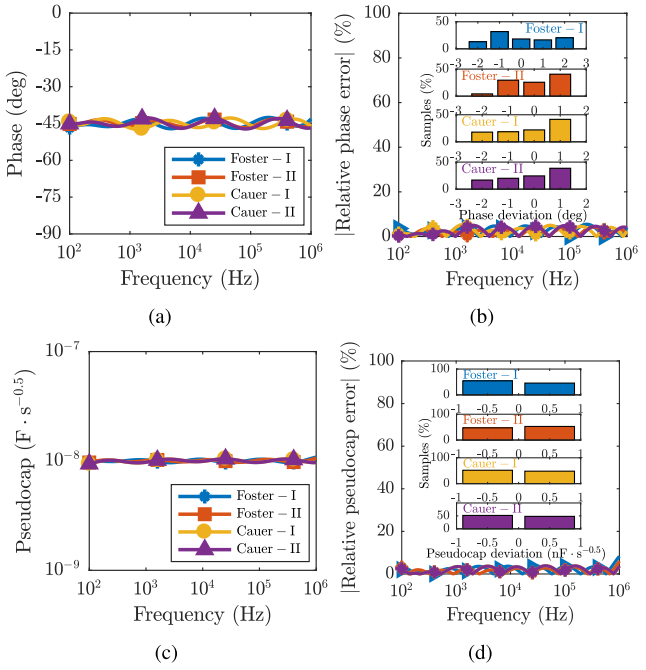

FIGURE 8. (a) Simulated phase and (b) relative phase errors and corresponding normalized histograms (%) of phase angle deviation from CPA as an inset, (c) pseudocapacitance responses, (d) relative pseudocapacitance errors and corresponding normalized histograms (%) of pseudocapacitance deviation from CPA as an inset, respectively, of four RC networks optimized using GA. Responses are optimized in the frequency range of 100 Hz–1 MHz.

range, operate up to a maximum of 5 GHz. In addition, this frequency range is inversely proportional to the resistance values. For instance, a 100 Ω resistor works until 8 GHz, whereas a 1 kΩ resistor has a constant zero-degree phase response up to 800 MHz and so forth. At high frequencies, the transmission line effect becomes dominant; therefore, we maintain the distance between passive elements the least. Despite the above mentioned limitations, we obtained the results until 1 GHz with low phase angle deviations as shown in Figs. 6(a)–(c).

MC analysis was performed in OrCAD PSpice® simulation software with 0402 kit resistors [60] and capacitors [62] with tolerance according to their datasheets, and 200 runs. The histogram shown in Fig. 7 demonstrates the variation of the phase at 30 MHz with values used in Fig. 6(a). The mean value with standard deviation 0.793 is −44.8853°, which is again very close to the theoretical value −45°.

One of the advantage of the proposed GA to design FOC is its suitability for any RC ladder topology, such as Cauer-I, Cauer-II, or Foster-I. In general, by replacing the admittance function of the desired topology, it is possible to determine the required resistance and capacitance values to build an FOC with desirable electrical properties. Notably, the list of admittances of listed networks can be found in Table 1. Fig. 8 shows the phase and pseudocapacitance responses with corresponding relative errors and normalized histograms (%) of deviations of four RC topologies while the target phase, pseudocapacitance, and frequency bandwidth are set to −45°, 10 nF·s$^{-0.5}$, and 4 decades in the frequency range of 100 Hz − 1 MHz, respectively. The largest deviation between the desired and simulated phase values in all topologies is up to ±2.5° with low pseudocapacitance deviation.

IV. OPTIMIZATION AND VERIFICATION OF FOI

The most popular technique to mimic an inductor is using a GIC employing Op-Amps, resistors, and capacitors [19],

TABLE 3. Comparison of simulation and measurement results of used methods for FOC design.

Topology	Method	No. of Branches	No. of Capacitors	No. of Resistors	|CPA Deviation| (°)	BW (decades)	FoM (°)
Foster-II	Oustaloup (Fig. 2(c) (simul.)	5	5	6	5	2.1	7.64×10^{-3}
	CFE (Fig. 2(c) (simul.)	5	5	6	5	2.35	8.55×10^{-3}
	This work (Fig. 2(c) (simul.)	5	5	6	2.4	4	30.3×10^{-3}
Valsa	RA (Fig. 5) (meas.)	5	6	6	5	3.8	12.67×10^{-3}
	This work (Fig. 5) (meas.)	5	6	6	2.1	4.7	37.3×10^{-3}
	This work (Fig. 6(a)) (meas.)	5	6	6	0.87	3	57.47×10^{-3}

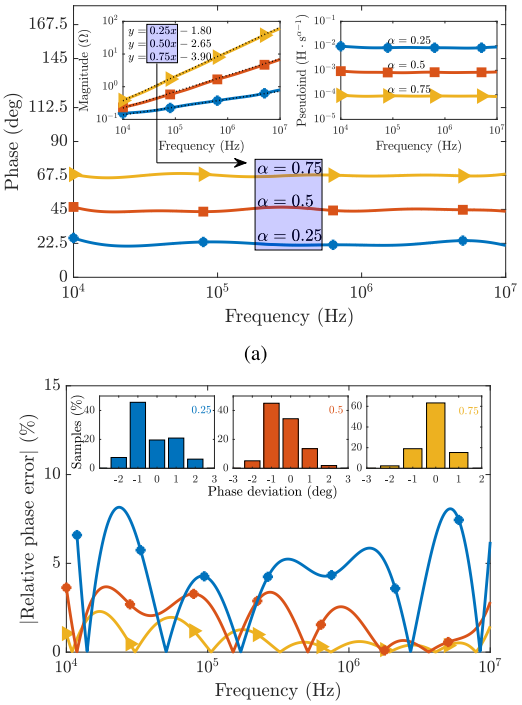

FIGURE 9. Numerical simulation results of five-branches Valsa RL network using 0603 kit R and L values for FOI design: (a) phase, pseudoinductance, and magnitude responses, (b) relative phase errors and corresponding normalized histograms (%) of three different orders in the frequency range of 10 kHz–10 MHz.

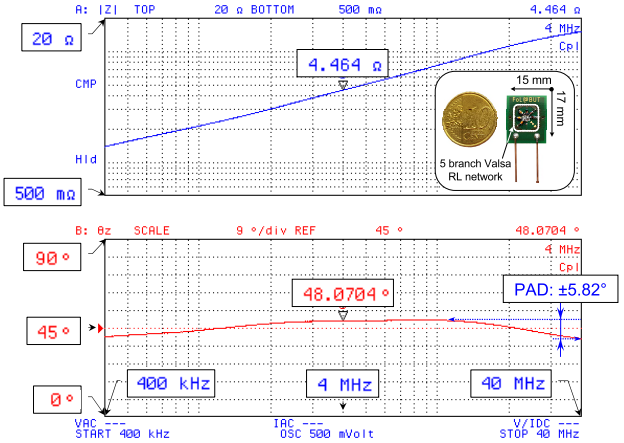

FIGURE 10. Measurement results of an $\alpha = 0.5$ order FOI from Fig. 9 and the fabricated device with dimensions of 15 mm × 17 mm as in inset (blue line - impedance response; red line - phase response).

[20], [33], [45]–[47], [49]– [52]. However, the performances of these GIC-based active inductance simulators often suffer from the non-idealities of Op-Amps. Therefore, this section deals with the optimal emulation of an FOI for the first time in the literature. The FOI design using the GA is studied numerically and experimentally verified.

A. OPTIMIZATION OF VALSA STRUCTURE FOR FOI DESIGN

The Valsa RC network in Table 1 is modified to an RL-type structure by replacing all capacitors with inductors as shown in corresponding figure. Its equivalent impedance function is given in Table 1, where n is the number of branches, R_0 is the initial resistor, L_0 is the initial inductor, R_i and L_i are the resistances and inductances of the i-th branch, respectively, while the fitness function is described as (1). The frequency response of five-branch FOIs with three different angles using 0603 kit R [59] and L [63] values is studied numerically and shown in Fig. 9. The pseudoinductances of orders $\alpha = \{0.25, 0.5, 0.75\}$ are 8.52 mH·s$^{-0.75}$, 834.62 μH·s$^{-0.5}$, and 89.62 μH·s$^{-0.25}$, which are constant with small deviations in the whole frequency range. Furthermore, the slope of magnitude in the inset of Fig. 9(a) shows that the inductive reactance (impedance) of the FOI increases as the supply frequency across it increases. To estimate the equivalent order α, the simulated magnitude responses are fitted to the function $\log_{10}|Z| = \alpha \log f + \log 10(2\pi)^{\alpha} L_{\alpha}$ using the linear least squares method. The equivalent equations from fitting the magnitude are provided inside Fig. 9(a). The maximum PAD and relative phase errors of the related orders are $\{\pm 1.84°, \pm 1.66°, \pm 1.55°\}$ and $\{\pm 8.16\%, \pm 3.68\%, \pm 2.29\%\}$, respectively, as depicted in Fig. 9(b). The operating frequency range is chosen between 10 kHz and 10 MHz because of the working frequency range of the 0603 kit ceramic chip inductors [63]. Considering that the maximum PAD is around ±2°, order of 0.25 is limited from 12 kHz. The used passive element values are listed in Appendix C.

Moreover, the behavior of an $\alpha = 0.5$ order FOI, numerically simulated in Fig. 9, was verified using the Agilent 4294A precision Impedance Analyzer. Standard calibration tests (open and short circuits) of the 16047E Test Fixture were performed to calibrate the instrument. During the experimental validation in the frequency range 400 kHz – 40 MHz (801 logarithmically spaced points in two decades),

TABLE 4. Passive element values for FOC using the Foster-II network and their performance characteristics.

Element	Fig. 2(a)			Fig. 2(c)		
	α = –0.5; C_α = 100 nF·s$^{-0.5}$					
	This work	CFE	Oustaloup	This work	CFE	Oustaloup
R_0 (Ω)	979.5 k	438.84 k	3.99 k	910 k	430 k	3.9 k
R_1 (Ω)	42.1 k	4.44 k	4.12 k	36 k	4.3 k	4.3 k
R_2 (Ω)	13.6 k	37.87 k	11.52 k	15 k	39 k	12 k
R_3 (Ω)	2.1 k	94.10 k	28.58 k	330 k	91 k	30 k
R_4 (Ω)	409.8 k	155.28 k	77.49 k	120 k	150 k	75 k
R_5 (Ω)	132.5 k	202 k	272.24 k	2.4 k	200 k	270 k
C_1 (F)	229.3 p	74.04 p	153.90 p	120 p	68 p	150 p
C_2 (F)	70.8 p	87.66 p	346.88 p	390 p	100 p	330 p
C_3 (F)	33.5 p	127 p	852.84 p	10 p	120 p	680 p
C_4 (F)	2.3 n	248.16 p	2.05n	0.47 p	270 p	2.2 n
C_5 (F)	722.5 p	913.85 p	3.69 n	120 p	1 n	3.3 n
	Operating frequency range					
	100 Hz – 1 MHz					
	Total resistance (Ω) / Total capacitance (F)					
	467.7 k / 3.17 n	932.53 k / 1.45 n	397.94 k / 7.09 n	1.41 M / 3.05 n	914.3 k / 1.56 n	395.2 k / 6.66 n
	Spread of resistance / capacitance					
	198.75 / 69.79	98.84 / 12.34	68.23 / 23.98	379.17 / 66.67	100 / 14.71	69.23 / 22
	Max. phase angle deviation (°) / relative phase error (%)					
	±1.8 / ±4.09	±25 / ±53.23	±25 / ±50.61	±2.4 / ±5.43	±40 / ±79.44	±30 / ±54.5
	Monte Carlo analysis: Variation of phase @ 10 kHz (mean / min / max (°))					
	–46.35 / –48 / –44.83	–45.06 / –46.45 / –43.68	–45 / –46.25 / –43.51	–46.74 / –47.7 / –45.61	–44.77 / –46.1 / –43.33	–43.02 / –44.41 / –41.41

TABLE 5. Passive element values for FOC using the Valsa network and their performance characteristics.

Element	Fig. 5 (α = –0.67)		Fig. 6 (α = –0.5)		
	This work	RA	This work (a)	This work (b)	This work (c)
R_0 (Ω)	10 M	24 k	1 k	330	250
R_1 (Ω)	24 k	10 k	1 k	250	10
R_2 (Ω)	4.7 k	3 k	221	330	100
R_3 (Ω)	110 k	820	221	50	25
R_4 (Ω)	2.4 M	270	250	500	200
R_5 (Ω)	470 k	75	20	221	221
R_6 (Ω)	–	–	1 k	20	330
C_0 (F)	7 p	1 n	0.1 p	4.7 p	1.5 p
C_1 (F)	18 p	10 n	100 p	68 p	2.7 p
C_2 (F)	10 p	4.7 n	68 p	8 p	8 p
C_3 (F)	39 p	3.3 n	12 p	15 p	6 p
C_4 (F)	200 p	1.5 n	12 p	12 p	12 p
C_5 (F)	91 p	0.82 n	22 p	15 p	6.8 p
C_6 (F)	–	–	100 p	7 p	100 p
	Operating frequency range				
	100 Hz – 10 MHz		1 MHz – 100 MHz	5 MHz – 500 MHz	50 MHz – 1 GHz
	Total resistance (Ω) / Total capacitance (F)				
	13.01 M / 365 p	38.17 k / 21.32 n	3.71 k / 314.1 p	1.7 k / 129.7 p	1.14 k / 137 p
	Spread of resistance / capacitance				
	416.67 / 28.57	320 / 12.2	50 / 1000	25 / 14.47	33 / 66.67
	Max. phase angle deviation (°) / relative phase error (%) Note: *100 Hz – 5 MHz				
	±2.1* / ±4.04*	±74.7 / ±124.51	±0.87 / ±1.94	±1.82 / ±4.63	±1.94 / ±4.58
	Monte Carlo analysis: Variation of phase (mean / min / max (°))				
	@ 30 kHz: –60.08 / –62.93 / –57.39	@ 30 kHz: –60.29 / –62.13 / –57.78	@ 30 MHz: –44.98 / –46.67 / –46.23	@ 60 MHz: –45.54 / –46.84 / –43.89	@ 400 MHz: –45.24 / –46.88 / –43.88

TABLE 6. Passive element values for FOI using the RL network and their performance characteristics.

Element	Fig. 9 (This work – Valsa network)			Fig. 13 (α = 0.5)			
	α = 0.25 L_α = 8.52 mH·s$^{-0.75}$	α = 0.5 L_α = 834.62 μH·s$^{-0.5}$	α = 0.75 L_α = 896.23 μH·s$^{-0.25}$	Foster-I L_α = 8 mH·s$^{-0.5}$	Foster-II L_α = 1 mH·s$^{-0.5}$	Cauer-I L_α = 4.78 mH·s$^{-0.5}$	Cauer-II L_α = 4.84 mH·s$^{-0.5}$
R_0 (Ω)	1	15	6.80 k	1	16	1	1 k
R_1 (Ω)	1	1	1	18	2.2	5.6	24
R_2 (Ω)	1	10	30 k	6.8	1	13	8.2
R_3 (Ω)	1	1	7.5	120	6.8	33	3
R_4 (Ω)	1	1.2	36	1.8	1	120	470 k
R_5 (Ω)	1	3.9	110	1	1	180 k	1
L_0 (H)	6.80 μ	6.80 μ	7.80 μ	–	–	–	–
L_1 (H)	270 n	6.80 μ	7.80 μ	1.5 μ	820 n	7.8 μ	360 n
L_2 (H)	3.30 μ	220 n	27 n	3.9 μ	3.3 μ	2.7 μ	1.8 μ
L_3 (H)	36 n	6.8 μ	5.60 μ	820 n	270 n	1.2 μ	4.7 μ
L_4 (H)	1.50 μ	1.2 μ	3.90 μ	7.8 μ	7.8 μ	470 n	6.8 μ
L_5 (H)	3.90 μ	470 n	1.50 μ	7.8 μ	7.8 μ	33 n	7.8 μ
	Operating frequency range						
	10 kHz – 10 MHz						
	Total resistance (Ω) / Total inductance (H)						
	6 / 15.81 μ	32.1 / 22.29 μ	36.96 k / 26.63 μ	149 / 21.82 μ	27 / 20 μ	180.17 k / 12.2 μ	471.04 k / 21.46 μ
	Spread of resistance / inductance						
	1 / 188.9	15 / 30.91	30 k / 288.89	120 / 9.51	16 / 2.89	180 k / 236	470 k / 21.67
	Max. phase angle deviation ($^\circ$) / relative phase error (%) Note: *12 kHz – 10 MHz						
	$\pm$1.84* / $\pm$8.16*	$\pm$1.66 / $\pm$3.68	$\pm$1.55 / $\pm$2.29	$\pm$1.9 / $\pm$4.22	$\pm$2.44 / $\pm$4.26	$\pm$20.04 / $\pm$44.54	$\pm$3.91 / $\pm$8.69
	Monte Carlo analysis: Variation of phase (mean / min / max ($^\circ$))						
	@ 300 kHz: 21.45 / 20.58 / 22.37	@ 3 MHz: 45.2 / 43.79 / 46.71	@ 300 kHz: 67.26 / 64.55 / 69.4	@ 100 kHz: 45.16 / 43.99 / 46.42	@ 100 kHz: 45.7 / 44.78 / 46.92	@ 300 kHz: 44.81 / 42.47 / 46.97	@ 300 kHz: 45.53 / 42.97 / 47.73

a sinusoidal input signal with a default AC voltage of 500 mV and a frequency of 1 MHz was applied, while one of terminals was grounded. The measurement results and a photograph of the fabricated device with dimensions of 15 mm $\times$ 17 mm are depicted in Fig. 10. The measured PAD in two decades of the frequency range of our interest is $\pm 5.82^\circ$.

In addition to an $\alpha = 0.5$ order FOI, a MC statistical analysis was also performed in the OrCAD PSpice® simulation software. The passive element tolerances according to 0603 kit datasheets [59], [63] and 200 runs were set to observe affects due to manufacturing processes. The histogram shown in Fig. 11 demonstrates the variation of the phase at 3 MHz. The mean value with standard deviation 0.49 is 45.1964°, which is very close to the theoretical value 45° confirming that the proposed network has low sensitivity characteristic on passive components.

In addition, for the first time in the literature, the Foster-I, Foster-II, Cauer-I, and Cauer-II type of RL networks are also studied. The impedance function of all networks optimized using GA are given in Table 1. Fig. 12 shows the phase and pseudoinductance responses with corresponding relative errors and normalized histograms (%) of deviations of four RL topologies. The target phase and frequency bandwidth are set to 45° and 3 decades in the frequency range of 10 kHz – 10 MHz, respectively, with no pseudoinductance

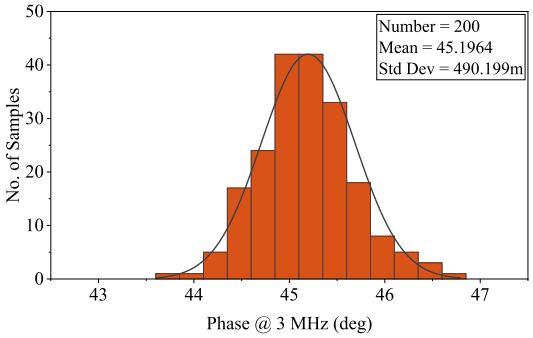

FIGURE 11. Monte Carlo analysis: Phase variation at 3 MHz of the Valsa RL network optimized using GA ($\alpha = 0.5$ order FOI with values used in Figs. 9 and 10).

specification to obtain the best result. In summary, the minimal error is obtained with Foster-I structure while the least spread of passive element values are observed with the Foster-II. The detailed analysis including MC results for all studied networks is presented in Appendix C.

V. BRIEF DISCUSSION OF RESULTS

Table 3 compares the performance of RC networks built using Oustaloup, CFE, RA, and the GA. For instance, for the Foster-II network composed of the same number of

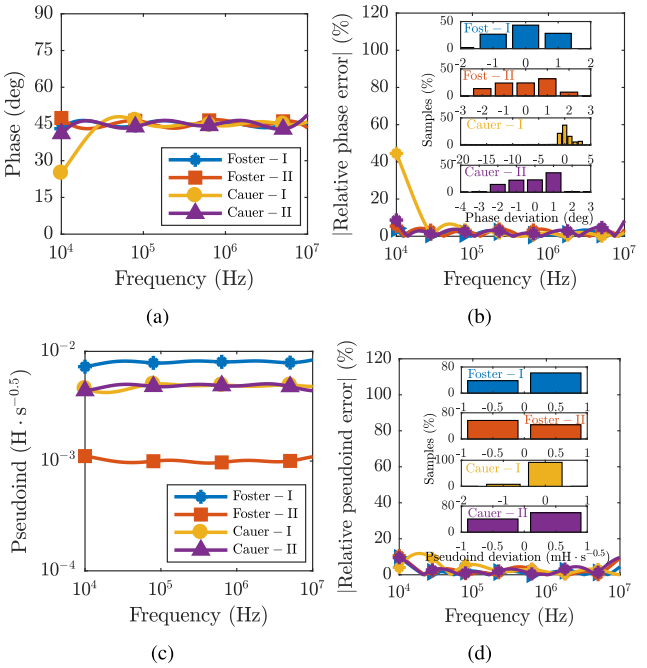

FIGURE 12. (a) Simulated phase responses, (b) relative phase errors and corresponding normalized histograms (%) of phase angle deviation from CPA as an inset, (c) pseudoinductances responses, and (d) relative pseudoinductances errors and corresponding normalized histograms (%) of pseudoinductances deviation from CPA as an inset, respectively, of different RL networks optimized using GA for FOI design. Impedance and phase responses are optimized in the frequency range of 10 kHz–10 MHz.

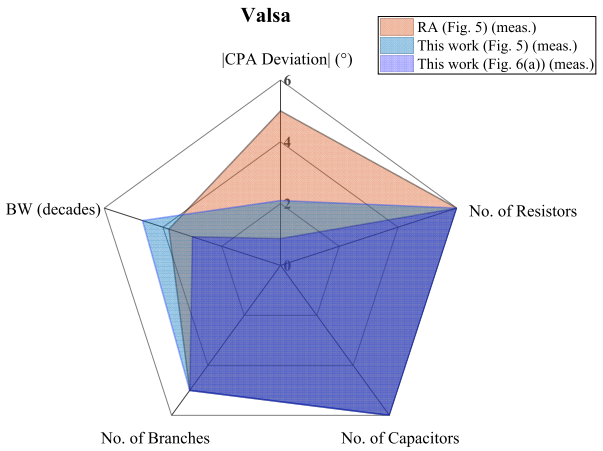

FIGURE 13. Radar chart showing an evaluation of Valsa RC structure results from Table 3.

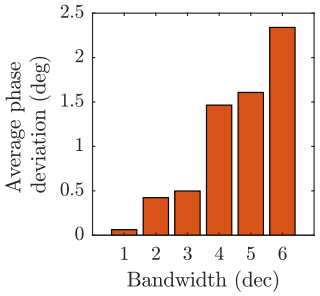

FIGURE 14. Numerical study of five-branches RC networks using random R and C values and plot of average phase angle deviation of an order of $\alpha = -0.5$ by increasing the operation bandwidth from 100 Hz up to 100 MHz.

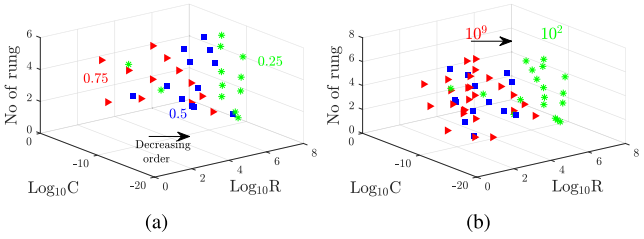

FIGURE 15. (a) Order and (b) frequency effect on R and C values on each rung of the Foster-II and Valsa structures for FOC design.

branches, the performance of the GA is compared with that of Oustaloup and CFE. The results obtained with the GA have the lowest PAD in a wider frequency range than Oustaloup and CFE. To provide the overall performance evaluation, a numeric Figure of Merit (FoM) value is calculated as:

$$\text{FoM} = \frac{\text{BW}}{\text{No. of Branches} \times \text{No. of Cap.} \times \text{No. of Res.} \times |\text{CPA Dev.}|}. \quad (2)$$

Notably, the FoM in our study for Foster-II network using the GA was 30.3×10^{-3}, which is the largest value. An improvement of approximately 396% over the Oustaloup and 354% over the CFE was achieved using the same number of elements and least CPA deviation in a wider bandwidth. In the same manner, the Valsa structure is compared between the RA and GA. Evidently, the GA provides a wider bandwidth than RA with lower CPA error. Moreover, the FoM shows significant improvements to the Valsa network with the GA (294% in case of Fig. 5 results). To comprehensively evaluate the performance of the Valsa structure using the RA and GA in Table 3, a radar chart is depicted in Fig. 13, which shows that a smaller area of pentagon provides superior performance (for instance, the GA in Fig. 6(a)). On the other hand, the error increases by increasing the bandwidth while maintaining the five branches as default (see numerical study in depicted in Fig. 14). It is clear that the phase angle deviation is less than $\pm 2.3°$ even with 6 decades of operation (from 100 Hz up to 100 MHz).

The performance of RC network optimizations is primarily compared through the utilization of the results in Appendix A and Appendix B. Here, total and spread of resistances and capacitances, phase angle deviation, relative phase error, and MC analysis for all networks are given. According to these, the GA generally provides the minimum total capacitance value and can be limited in any range of the designer's choice. Furthermore, as the order increases, the total capacitance increases and the resistance decreases, as shown in Fig. 15(a). Maintaining the order constant and increasing the capacitance value provides the same results as in the previous case. The

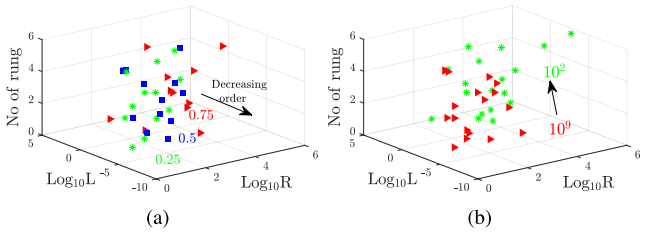

FIGURE 16. (a) Order and (b) frequency effect on *R* and *L* values on each rung of the Valsa structures for FOI design.

frequency effect on the values is shown in Fig. 15(b). At high frequencies, small R and C values are used (as also seen in Appendix B), whereas larger passive values are used at low frequencies. This fact can be explained by the dissipation factor (DF) expressed as $\mathrm{DF} = \mathrm{ESR}/X_C$, where ESR and X_C denote the equivalent series resistance and capacitors reactance, respectively, or as a tangent of the loss angle [64].

Fig. 16 shows the distribution of R and L values depending on an order and the frequency range for FOI design. Different to the FOC evaluation, resistance and inductance vary linearly with an order. It is also clear from Appendix C that an increasing FOI order has the effect of increasing passive values. This result can be explained by the quality factor (Q) definition $Q = X_L/R$, where X_L is the inductive reactance and R is the DC resistance [65]. Maintaining the Q constant, increasing an order (effecting X_L) has the effect of increasing the R. At low frequencies and within limits, both passive values become much greater than their equivalents at high frequencies.

VI. CONCLUSION

In this study, a new approach for the design of an FOE, mainly from the Foster-II and Valsa structures, with desired properties was introduced. The mixed integer-order GA was used to determine the optimal phase response with minimum phase angle deviation in a defined frequency range. The values of the passive elements have been optimized in accordance with the commercially available IEC 60063 compliant kits. Therefore, the introduced approach offers enormous freedom to design RC/RL networks without making any value adjustments, which could lead to degeneration of FOE performance during measurements. Furthermore, designers can obtain the optimal phase and impedance response at low-, mid-, and high frequencies with wide bandwidths and low phase errors with minimum total passive element. The results demonstrated excellent performance as well as adaptability for application to various types of structure, such as Cauer-I, Cauer-II, and Foster-I either for FOC or FOI design, which was carried out for the first time in the literature. All these features make this approach strong and beneficial analogue designer. It is also important to note that the proposed approach outperformed other approximations or algorithms such as the recursive algorithm [15], Oustaloup's approximations [35], graphical method [20], meta-heuristic algorithms [44], and the design using bilinear sections [47]. In other words, a fifth-order approximation of FOE using GA shows better performance than for example fourteenth-[15] or ninth-order [20] approximations. In addition, during our research, we found that there is a connection between the FOE and the equivalent circuit model of the inductors and electrolytic capacitors. Thus, more accurate models of these components can be developed in the future.

APPENDIX A

See Table 4.

APPENDIX B

See Table 5.

APPENDIX C

See Table 6.

ACKNOWLEDGMENT

For the research, infrastructure of the SIX Center was used. *(Aslihan Kartci and Agamyrat Agambayev contributed equally to this work.)*

REFERENCES

[1] M. D. Ortigueira, "An introduction to the fractional continuous-time linear systems: The 21st century systems," *IEEE Circuits Syst. Mag.*, vol. 8, no. 3, pp. 19–26, Sep. 2008.

[2] A. S. Elwakil, "Fractional-order circuits and systems: An emerging interdisciplinary research area," *IEEE Circuits Syst. Mag.*, vol. 10, no. 4, pp. 40–50, Nov. 2010.

[3] H. Sun, Y. Zhang, D. Baleanu, W. Chen, and Y. Chen, "A new collection of real world applications of fractional calculus in science and engineering," *Commun. Nonlinear Sci. Numer. Simul.*, vol. 64, pp. 213–231, Apr. 2018.

[4] A. K. Gil'mutdinov, P. A. Ushakov, and R. El-Khazali, *Fractal Elements and their Applications*. Cham, Switzerland: Springer, 2017.

[5] A. G. Radwan and K. N. Salama, "Passive and active elements using fractional $L_\beta C_\alpha$ circuit," *IEEE Trans. Circuits Syst. I, Reg. Papers*, vol. 58, no. 10, pp. 2388–2397, Oct. 2011.

[6] A. S. Ali, A. G. Radwan, and A. M. Soliman, "Fractional order Butterworth filter: Active and passive realizations," *IEEE J. Emerg. Sel. Topics Circuits Syst.*, vol. 3, no. 3, pp. 346–354, Sep. 2013.

[7] J. Jerabek, R. Sotner, J. Dvorak, J. Polak, D. Kubanek, N. Herencsar, and J. Koton, "Reconfigurable fractional-order filter with electronically controllable slope of attenuation, pole frequency and type of approximation," *J. Circuits, Syst. Comput.*, vol. 26, no. 10, pp. 1750157-1–1750157-21, 2017.

[8] A. G. Radwan, A. S. Elwakil, and A. M. Soliman, "Fractional-order sinusoidal oscillators: Design procedure and practical examples," *IEEE Trans. Circuits Syst. I, Reg. Papers*, vol. 55, no. 7, pp. 2051–2063, Aug. 2008.

[9] A. Kartci, N. Herencsar, J. Koton, L. Brancik, K. Vrba, G. Tsirimokou, and C. Psychalinos, "Fractional-order oscillator design using unity-gain voltage buffers and Otas," in *Proc. 60th IEEE Int. Midwest Symp. Circuits Syst. (MWSCAS)*, Boston, MA, USA, Aug. 2017, pp. 555–558.

[10] A. S. Elwakil, A. Agambayev, A. Allagui, and K. N. Salama, "Experimental demonstration of fractional-order oscillators of orders 2.6 and 2.7," *Chaos, Solitons Fractals*, vol. 96, pp. 160–164, Mar. 2017.

[11] A. Agambayev, A. Kartci, A. H. Hassan, N. Herencsar, H. Bagci, and K. N. Salama, "Fractional-order Hartley oscillator," in *Proc. 2018 14th Conf. Ph.D. Res. Microelectron. Electron. (PRIME)*, Prague, Czech Republic, 2018, pp. 45–48.

[12] M. Chen, S.-Y. Shao, P. Shi, and Y. Shi, "Disturbance-observer-based robust synchronization control for a class of fractional-order chaotic systems," *IEEE Trans. Circuits Syst. II, Exp. Briefs*, vol. 64, no. 4, pp. 417–421, Apr. 2017.

[13] G. W. Bohannan, "Analog fractional order controller in temperature and motor control applications," *J. Vibrat. Control*, vol. 14, nos. 9–10, pp. 1487–1498, 2008.

[14] A. Tepljakov, E. A. Gonzalez, E. Petlenkov, J. Belikov, C. A. Monje, and I. Petras, "Incorporation of fractional-order dynamics into an existing PI/PID DC motor control loop," *ISA Trans.*, vol. 60, pp. 262–273, Jan. 2016.
[15] O. Domansky, R. Sotner, L. Langhammer, J. Jerabek, C. Psychalinos, and G. Tsirimokou, "Practical design of RC approximants of constant phase elements and their implementation in fractional-order PID regulators using CMOS voltage differencing current conveyors," *Circuits, Syst. Signal Process.*, vol. 38, no. 4, pp. 1520–1546, 2019.
[16] T. J. Freeborn, "A survey of fractional-order circuit models for biology and biomedicine," *IEEE J. Emerg. Sel. Topics Circuits Syst.*, vol. 3, no. 3, pp. 416–424, Sep. 2013.
[17] Y. Ma, X. Zhou, B. Li, and H. Chen, "Fractional modeling and SOC estimation of lithium-ion battery," *IEEE/CAA J. Automatica Sinica*, vol. 3, no. 3, pp. 281–287, Jul. 2016.
[18] N. A.-Z. R.-Smith, A. Kartci, and L. Brančík, "Application of numerical inverse Laplace transform methods for simulation of distributed systems with fractional-order elements," *J. Circuits, Syst. Comput.*, vol. 27, no. 11, pp. 1850172-1–1850172-25, 2018.
[19] V. P. Sarathi, G. Uma, and M. Umapathy, "Realization of fractional order inductive transducer," *IEEE Sensors J.*, vol. 18, no. 21, pp. 8803–8811, Nov. 2018.
[20] X. Chen, Y. Chen, B. Zhang, and D. Qiu, "A modeling and analysis method for fractional-order DC–DC converters," *IEEE Trans. Power Electron.*, vol. 32, no. 9, pp. 7034–7044, Sep. 2017.
[21] S. Singh and M. S. Hashmi, "Exploring fractional order elements for single and dual band impedance matching for RF applications," in *Proc. Int. Conf. Signal Process. Commun.(SPCOM)*, Bangalore, India, 2016, pp. 1–5.
[22] A. G. Radwan and K. N. Salama, "Fractional-order RC and RL circuits," *Circuits, Syst., Signal Process.*, vol. 31, no. 6, pp. 1901–1915, 2012.
[23] A. Adhikary, P. Sen, S. Sen, and K. Biswas, "Design and performance study of dynamic fractors in any of the four quadrants," *Circuits, Syst., Signal Process.*, vol. 35, no. 6, pp. 1909–1932, Jun. 2016.
[24] A. Agambayev, K. H. Rajab, A. H. Hassan, M. Farhat, H. Bagci, and K. N. Salama, "Towards fractional-order capacitors with broad tunable constant phase angles: Multi-walled carbon nanotube-polymer composite as a case study," *J. Phys. D, Appl. Phys.*, vol. 51, no. 6, p. 065602, pp. 1–6, 2018.
[25] A. Kartci, A. Agambayev, N. Herencsar, and K. N. Salama, "Series-, parallel-, and inter-connection of solid-state arbitrary fractional-order capacitors: Theoretical study and experimental verification," *IEEE Access*, vol. 6, pp. 10933–10943, 2018.
[26] A. Agambayev, S. Patole, M. Farhat, A. Elwakil, H. Bagci, and K. N. Salama, "Ferroelectric fractional-order capacitors," *ChemElectroChem*, vol. 4, no. 11, pp. 2807–2813, 2017.
[27] A. Agambayev, S. Patole, H. Bagci, and K. N. Salama, "Tunable fractional-order capacitor using layered ferroelectric polymers," *AIP Adv.*, vol. 7, no. 9, pp. 095202-1–095202-8, 2017.
[28] K. Biswas, S. Sen, and P. K. Dutta, "Realization of a constant phase element and its performance study in a differentiator circuit," *IEEE Trans. Circuits Syst. II, Exp. Briefs*, vol. 53, no. 9, pp. 802–806, Sep. 2006.
[29] M. S. Krishna, S. Das, K. Biswas, and B. Goswami, "Fabrication of a fractional order capacitor with desired specifications: A study on process identification and characterization," *IEEE Trans. Electron Devices*, vol. 58, no. 11, pp. 4067–4073, Nov. 2011.
[30] G. Tsirimokou, C. Psychalinos, A. S. Elwakil, and K. N. Salama, "Electronically tunable fully integrated fractional-order resonator," *IEEE Trans. Circuits Syst. II, Exp. Briefs*, vol. 65, no. 2, pp. 166–170, Feb. 2018.
[31] G. Carlson and C. Halijak, "Approximation of Fractional Capacitors (1/s)^(1/n) by a regular Newton process," *IEEE Trans. Circuit Theory*, vol. 11, no. 2, pp. 210–213, Jun. 1964.
[32] K. Matsuda and H. Fujii, "H∞ optimized wave absorbing control: Analytical and experimental result," *J. Guid., Control, Dyn.*, vol. 16, no. 3, pp. 1146–1153, 1993.
[33] R. El-Khazali, "On the biquadratic approximation of fractional-order Laplacian operators," *Analog Integr. Circuits Signal Process.*, vol. 82, no. 3, pp. 503–517, 2015.
[34] G. Maione, "High-speed digital realizations of fractional operators in the delta domain," *IEEE Trans. Autom. Control*, vol. 56, no. 3, pp. 697–702, Mar. 2011.
[35] A. Oustaloup, F. Levron, B. Mathieu, and F. M. Nanot, "Frequency-band complex noninteger differentiator: Characterization and synthesis," *IEEE Trans. Circuits Syst. I, Fundam. Theory Appl.*, vol. 47, no. 1, pp. 25–39, Jan. 2000.
[36] G. Tsirimokou, C. Psychalinos, and A. S. Elwakil, *Design of CMOS Analog Integrated Fractional-Order Circuits—Applications in Medicine and Biology*. Cham, Switzerland: Springer, 2017.
[37] J. Valsa and J. Vlach, "RC models of a constant phase element," *Int. J. Circuit Theory Appl.*, vol. 41, no. 1, pp. 59–67, 2013.
[38] J. A. T. Machado, "Discrete-time fractional-order controllers," *Fractional Calculus Appl. Anal.*, vol. 4, no. 1, pp. 47–66, 2001.
[39] Z. Gao and X. Liao, "Rational approximation for fractional-order system by particle swarm optimization," *Nonlinear Dyn.*, vol. 67, no. 2, pp. 1387–1395, 2012.
[40] J. A. T. Machado, A. M. Galhano, A. M. Oliveira, and J. K. Tar, "Optimal approximation of fractional derivatives through discrete-time fractions using genetic algorithms," *Commun. Nonlinear Sci. Numer. Simul.*, vol. 15, no. 3, pp. 482–490, 2010.
[41] Y. Q. Chen and K. L. Moore, "Discretization schemes for fractional-order differentiators and integrators," *IEEE Trans. Circuits Syst. I, Fundam. Theory Appl.*, vol. 49, no. 3, pp. 363–367, Mar. 2002.
[42] B. M. Vinagre, I. Podlubny, A. Hernandez, and V. Feliu, "Some approximations of fractional order operators used in control theory and applications," *Fractional Calculus Appl. Anal.*, vol. 3, no. 3, pp. 231–248, 2000.
[43] Y.-F. Pu, "Measurement units and physical dimensions of fractance—Part I: Position of purely ideal fractor in Chua's axiomatic circuit element system and fractional-order reactance of fractor in its natural implementation," *IEEE Access*, vol. 4, pp. 3379–3397, 2016.
[44] A. M. AbdelAty, A. S. Elwakil, A. G. Radwan, C. Psychalinos, and B. J. Maundy, "Approximation of the fractional-order Laplacian s^{α} as a weighted sum of first-order high-pass filters," *IEEE Trans. Circuits Syst. II, Exp. Briefs*, vol. 65, no. 8, pp. 1114–1118, Aug. 2018.
[45] G. Tsirimokou, A. Kartci, J. Koton, N. Herencsar, and C. Psychalinos, "Comparative study of discrete component realizations of fractional-order capacitor and inductor active emulators," *J. Circuits, Syst. Comput.*, vol. 27, no. 11, pp. 1850170-1–1850170-26, 2018.
[46] C. Muñiz-Montero, L. V. García-Jiménez, L. A. Sánchez-Gaspariano, C. Sánchez-López, V. R. González-Díáz, and E. Tlelo-Cuautle, "New alternatives for analog implementation of fractional-order integrators, differentiators and PID controllers based on integer-order integrators," *Nonlinear Dyn.*, vol. 90, no. 1, pp. 241–256, 2017.
[47] R. Sotner, J. Jerabek, A. Kartci, O. Domansky, N. Herencsar, V. Kledrowetz, B. B. Alagoz, and C. Yeroglu, "Electronically reconfigurable two-path fractional-order PI/D controller employing constant phase blocks based on bilinear segments using CMOS modified current differencing unit," *Microelectron. J.*, vol. 86, pp. 114–129, 2019.
[48] D. Sierociuk, I. Podlubny, and I. Petras, "Experimental evidence of variable-order behavior of ladders and nested ladders," *IEEE Trans. Control Syst. Technol.*, vol. 21, no. 2, pp. 459–466, Mar. 2013.
[49] K. Biswas, G. Bohannan, R. Caponetto, A. M. Lopes, and J. A. T. Machado, *Fractional-Order Devices*. Cham, Switzerland: Springer, 2017.
[50] A. Adhikary, S. Sen, and K. Biswas, "Practical realization of tunable fractional order parallel resonator and fractional order filters," *IEEE Trans. Circuits Syst. I, Reg. Papers*, vol. 63, no. 8, pp. 1142–1151, Aug. 2016.
[51] A. Adhikary, S. Choudhary, and S. Sen, "Optimal design for realizing a grounded fractional order inductor using GIC," *IEEE Trans. Circuits Syst. I, Reg. Papers*, vol. 65, no. 8, pp. 2411–2421, Aug. 2018.
[52] N. Herencsar, "Balanced-output CCCFOA and its utilization in grounded inductance simulator with various orders," in *Proc. 41st Int. Conf. Telecommun. Signal Process. (TSP)*, Athens, Greece, 2018, pp. 188–191.
[53] W. Du, L. Tong, and Y. Tang, "Metaheuristic optimization-based identification of fractional-order systems under stable distribution noises," *Phys. Lett. A*, vol. 382, no. 34, pp. 2313–2320, 2018.
[54] E. S. Pires, J. T. Machado, P. B. de Moura Oliveira, J. B. Cunha, and L. Mendes, "Particle swarm optimization with fractional-order velocity," *Nonlinear Dyn.*, vol. 61, nos. 1–2, pp. 295–301, 2010.
[55] D. Yousri, A. M. AbdelAty, A. G. Radwan, A. S. Elwakil, and C. Psychalinos, "Comprehensive comparison based on meta-heuristic algorithms for approximation of the fractional-order Laplacian s^{α} as a weighted sum of first-order high-pass filters," *Microelectron. J.*, vol. 87, pp. 110–120, May 2019.
[56] X.-S. Yang, "Flower pollination algorithm for global optimization," in *Proc. 11th Int. Conf. Unconventional Comput. Natural Comput. (UCNC)*, Orlean, France, 2012, pp. 240–249.
[57] Y. Shi and R. Eberhart, "A modified particle swarm optimizer," in *Proc. IEEE Int. Conf. Evol. Comput.*, Anchorage, AK, USA, May 1998, pp. 69–73.

[58] P. C. Chu and J. E. Beasley, "A genetic algorithm for the generalised assignment problem," *Comput. Oper. Res.*, vol. 24, no. 1, pp. 17–23, 1997.
[59] *Datasheet: YAGEO Corporation 'General Purpose Chip Resistors RC_L Series RC-0603-FR-07 E96 1R-10M 1% Kit'* document, Mar. 2018. [Online]. Available: https://goo.gl/V3D5Jn
[60] *Datasheet: Vishay Intertechnology Inc. High Frequency 50 GHz Thin Film 0402 Chip Resistor*, document 53014, Feb. 2018. [Online]. Available: https://www.vishay.com/docs/53014/ch.pdf
[61] *Datasheet: muRata Manufacturing Co., Ltd. 'Chip Multilayer Ceramic Capacitors for General—GRM1885C1 Series 50Vdc C0G 0603 0.50pF-10nF Capacitor Kit'* document C02E.pdf, Nov. 2017. [Online]. Available: https://goo.gl/wFb535
[62] *Datasheet: Kemet Electronics Corporation 'HiQ-CBR Series, 0402 C0G Dielectric, Low ESR 6.3—500 VDC, 1 MHz 50 GHz (RF & Microwave)*, document C1030_C0G_CBR, 2018. [Online]. Available: https://goo.gl/fdpbQ8
[63] *Datasheet: Coilcraft, Inc. 'Magnetics for RF, Power, Filter and Data Applications—0603 Ceramic Inductors'*, document, 2018. [Online]. Available: https://www.coilcraft.com/pdfs/ShortFormCatalog.pdf
[64] W. J. Sarjeant, "Capacitors," *IEEE Trans. Electr. Insul.*, vol. 25, no. 5, pp. 861–922, Oct. 1990.
[65] F. Yuan, *CMOS Active Inductors and Transformers-Principle, Implementation, and Applications*. New York, NY, USA: Springer, 2008.

ASLIHAN KARTCI (S'15) received the M.S. degree in electronics from Yildiz Technical University, Turkey, in 2015. She is currently pursuing the Ph.D. degree with the Department of Radio Electronics, Brno University of Technology, Czech Republic. Her research interests include fractional-order analog integrated circuits with modern active elements and their application as oscillators and filters, general element simulator, numerical methods for analysis of electronic networks, and computer-aided methods for the simulation of electronic circuits for high-frequency applications.

AGAMYRAT AGAMBAYEV was born in Mary, Turkmenistan, in 1992. He received the B.S. degree in physics with double majoring in electrical and electronics engineering, in 2012 and the M.S. degree in biomedical engineering from Fatih University, Istanbul, Turkey, in 2014. He is currently pursuing the Ph.D. degree in electrical engineering with the King Abdullah University of Science and Technology, Thuwal, Saudi Arabia. His research interests include modeling, designing, and the application of the fractional-order circuit elements and nanocomposites for energy storage systems.

MOHAMED FARHAT received the Ph.D. degree in optics and electromagnetism from Aix-Marseille University and the master's degree in theoretical physics. He has authored more than 140 publications: 60 journal papers, 5 book chapters, 5 international patents, 4 proceedings, and 70 conference papers, with more than 2400 citations (h-index 24, from Google Scholar or ISI). He has also co-edited the book *Transformation Wave Physics: Electromagnetics, Elastodynamics and Thermodynamics* (Pan Stanford Publishing). He has organized several special sessions at the conferences Meta'13, Meta'14, Meta'15, Meta'16, Meta'17, and Meta'18. His research interests include plasmonics and metamaterials with applications spanning optics and acoustics waves. He is an Active Reviewer for many international journals in physics, including *Physical Review Letters* and *Nature Physics*.

NORBERT HERENCSAR (S'07–M'12–SM'15) received the M.S. and Ph.D. degrees in electronics and communication and teleinformatics from the Brno University of Technology (BUT), Brno, Czech Republic, in 2006 and 2010, respectively.

In 2013 and 2014, he was a Visiting Researcher with the Department of Electrical and Electronics Engineering, Bogazici University, Istanbul, Turkey, and also with the Department of Electronics and Communications Engineering, Dogus University, Istanbul. Since 2019, he has been a Visiting Professor with the Department of Electrical and Computer Engineering, University of Calgary, Canada. Since 2015, he has also been an Associate Professor with the Department of Telecommunications, BUT. Since 2006, he has been collaborating on numerous research projects supported by the Czech Science Foundation. He is currently the Science Communications Manager and an MC Member of the COST Action CA15225 Fractional-Order Systems—Analysis, Synthesis and Their Importance for Future Design. He has authored 82 articles published in SCI-E peer-reviewed journals and about 120 papers published in proceedings of international conferences. His research interests include analog electronics, current-mode circuits, and fractional-order systems synthesis.

He is a Senior Member of the IACSIT and IRED and a member of the IAENG, ACEEE, and RS. Since 2010, he has been the Deputy Chair of the International Conference on Telecommunications and Signal Processing (TSP) and organizing or TPC member of the AFRICON, ELECO, I^2MTC, ICUMT, IWSSIP, SET-CAS, MWSCAS, and ICECS conferences. In 2016, he was the General Co-Chair of the COST/IEEE-CASS Seasonal Training School in Fractional-Order Systems. Since 2017, he has been the General Co-Chair of the TSP. Since 2011, he has been contributing as a Guest Co-Editor to several special journal issues in *AEU—International Journal of Electronics and Communications*, *Radioengineering*, and *Telecommunication Systems*. Since 2014, 2017, and 2018, he has been serving as an Associate Editor of the *Journal of Circuits, Systems and Computers* (JCSC), IEEE Access, *IEICE Electronics Express* (ELEX), and an Editorial Board Member of the *Radioengineering*, *Elektronika ir Elektrotechnika*, and *Fractal and Fractional*, respectively. Since 2015, he has also been serving in the IEEE Czechoslovakia Section Executive Committee as a SP/CAS/COM Joint Chapter Chair.

LUBOMIR BRANCIK (M'00–SM'16) received the Ing. (M.Sc. equivalent) degree in microelectronics and the C.Sc. (Ph.D. equivalent) degree in measurements from the Brno University of Technology, Czech Republic, in 1985 and 1993, respectively, where he is currently a Professor of theoretical electrical engineering with the Department of Radio Electronics. From 2008 to 2010, he served as a Chair of the Czechoslovakia Section, IEEE. His research interests include numerical methods for the electrical engineering, computer-aided simulation, and signal integrity issues in electronic circuits.

HAKAN BAGCI (S'98–M'07–SM'14) received the B.S. degree in electrical and electronics engineering from Bilkent University, Ankara, Turkey, in 2001, and the M.S. and Ph.D. degrees in electrical and computer engineering from the University of Illinois at Urbana–Champaign (UIUC), Urbana, IL, USA, in 2003 and 2007, respectively.

From 1999 to 2001, he was an Undergraduate Researcher with the Computational Electromagnetics Group, Bilkent University. From 2001 to 2006, he was a Research Assistant with the Center for Computational Electromagnetics and Electromagnetics Laboratory, UIUC. From 2007 to 2009, he was a Research Fellow with the Radiation Laboratory, University of Michigan, Ann Arbor, MI, USA. Since 2009, he has been with the King Abdullah University of Science and Technology (KAUST), Thuwal, Saudi Arabia, where he is currently an Associate Professor of electrical engineering. He authored or coauthored 90 journal papers and 200 papers in conference proceedings. His research interests include various aspects of theoretical and applied computational electromagnetics with emphasis on well-conditioned frequency and time domain integral equation formulations and their discretization, hybrid time domain integral and differential equation solvers, accurate, stable, and efficient marching schemes for time domain solvers, stochastic characterization of electromagnetic field and wave interactions on complex geometries, and solution of two and three dimensional electromagnetic inverse scattering problem using signal processing techniques.

Dr. Bagci was a recipient of the 2008 International Union of Radio Scientists (URSI) Young Scientist Award and the 2004–2005 Interdisciplinary Graduate Fellowship from the Computational Science and Engineering Department, UIUC. His paper Fast and Rigorous Analysis of EMC/EMI Phenomena on Electrically Large and Complex Structures Loaded With Coaxial Cables was one of the three finalists (with honorable mention) for the 2008 Richard B. Schulz Best Transactions Paper Award given by the IEEE Electromagnetic Compatibility Society. He authored (as student) or coauthored (as student and advisor) 17 finalist/honorable mention papers in the student paper competitions at the 2005, 2008, 2010, 2014, 2015, 2016, 2017, 2018 IEEE Antennas and Propagation Society International Symposiums and the 2013, 2014, 2016, 2017, and 2018 Applied Computational Electromagnetics Society Conferences.

KHALED N. SALAMA (S'97–M'05–SM'10) received the B.S. degree from the Department Electronics and Communications, Cairo University, Cairo, Egypt, in 1997, and the M.S. and Ph.D. degrees from the Department of Electrical Engineering, Stanford University, Stanford, CA, USA, in 2000 and 2005, respectively. He was an Assistant Professor with the Rensselaer Polytechnic Institute, NY, USA, from 2005 to 2009. He joined the King Abdullah University of Science and Technology (KAUST), in 2009, where he is currently a Professor, and was the Founding Program Chair, until 2011. He is the Director of the sensors initiative a consortium of 9 universities [KAUST, MIT, UCLA, GATECH, MIT, UCLA, Brown University, Georgia Tech, TU Delft, Swansea University, the University of Regensburg, and the Australian Institute of Marine Science (AIMS)].

His work on CMOS sensors for molecular detection has been funded by the National Institutes of Health (NIH) and the Defense Advanced Research Projects Agency (DARPA), awarded the Stanford–Berkeley Innovators Challenge Award in biological sciences and was acquired by Lumina, Inc. He has authored 250 papers and 20 U.S. patents on low-power mixed-signal circuits for intelligent fully integrated sensors and neuromorphic circuits using memristor devices.